Interaction of Protegrin-1 with Lipid Bilayers: Membrane Thinning Effect

Hyunbum Jang,* Buyong Ma,* Thomas B. Woolf,† and Ruth Nussinov*‡
*Center for Cancer Research Nanobiology Program, SAIC-Frederick, Inc., NCI-Frederick, Frederick, Maryland 21702; †Department of Physiology, Johns Hopkins University, School of Medicine, Baltimore, Maryland 21205; and ‡Sackler Institute of Molecular Medicine, Department of Human Genetics and Molecular Medicine, Sackler School of Medicine, Tel Aviv University, Tel Aviv 69978, Israel

ABSTRACT Protegrins (PG) are important in defending host tissues, preventing infection via an attack on the membrane surface of invading microorganisms. Protegrins have powerful antibiotic abilities, but the molecular-level mechanisms underlying the interactions of their β-sheet motifs with the membrane are not known. Protegrin-1 (PG-1) is composed of 18 amino acids with a high content of basic residues and two disulfide bonds. Here we focused on the stability of PG-1 at the amphipathic interface in lipid bilayers and on the details of the peptide-membrane interactions. We simulated all-atom models of the PG-1 monomer with explicit water and lipid bilayers composed of both homogeneous POPC (palmitoyl-oleyl-phosphatidylcholine) lipids and a mixture of POPC/POPG (palmitoyl-oleyl-phosphatidylglycerol) (4:1) lipids. We observed that local thinning of the lipid bilayers mediated by the peptide is enhanced in the lipid bilayer containing POPG, consistent with experimental results of selective membrane targeting. The β-hairpin motif of PG-1 is conserved in both lipid settings, whereas it is highly bent in aqueous solution. The conformational dynamics of PG-1, especially the highly charged β-hairpin turn region, are found to be mostly responsible for disturbing the membrane. Even though the eventual membrane disruption requires PG-1 oligomers, our simulations clearly show the first step of the monomeric effects. The thinning effects in the bilayer should relate to pore/channel formation in the lipid bilayer and thus be responsible for further defects in the membrane caused by oligomer.

INTRODUCTION

Several hundreds of proteins/peptides are known to cause membrane damage and to lead to cell death. They are found in many organisms such as plants, insects, frogs, snakes, and humans. Many such peptides are used by nature as either host defense (antimicrobial peptides) or offense (toxins from spider and snake venom). Since the body produces peptides that act against its own cells, the cytotoxic peptides are involved in ''autocytotoxic'' conditions (1). In addition to the wild-type cytolytic peptides, synthetic peptides modified from naturally occurring cytolytic peptides can also be cytotoxic, with mutation-sensitive activities (2,3). The size of the protein ranges from a short peptide to several hundreds of amino acids. Both large proteins and small peptides share a common feature, the ability to create a leakage pathway for molecules and ions to cross lipid bilayers (4).

The monomeric structures of small cytolytic peptides can be classified into three groups: α-helix, β-sheet, and loop-strand. These peptides adopt totally different structures under different conditions, allowing the conformation to adjust to the surrounding environment. Most α-helical cytolytic peptides are largely random coil in solution and change to an α-helix within the membrane. The β-strand and loop-strand peptides often have disulfide S-S bond(s) that constrain the peptide conformation (5). Even though it is uncertain whether these disulfide bond-constrained peptides will have similar conformations in solution and in the membrane, it is commonly assumed that the disulfide bonds will keep the β-sheet structure unchanged. The most prominent characteristic of the small cytolytic peptides is that they are largely amphipathic, with hydrophobic and positively charged hydrophilic regions (with an excess of Lys and Arg residues). Positively charged residues can facilitate an initial contact between the peptides and the polyanionic sites in the membrane. Amphipathicity is essential for the membrane disruption effects by these peptides (5).

One of the best characterized β-sheet cytolytic peptide is protegrin. Native protegrins were originally purified from porcine leukocytes. There are five known porcine protegrins, PG-1–PG-5. These peptides share a common feature and conformation. Protegrin-1 (PG-1) forms the β-hairpin conformation, which is composed of 18 amino acids (RGGRL-CYCRR-RFCVC-VGR) with a high content of cysteine (Cys) and positively charged arginine (Arg) residues. Formation of two disulfide bonds between the cysteine residues in PG-1 is crucial for the peptide activity, since the activity can be restored by stabilizing the peptide structure (2). It was noted that the translocation ability of PG-1 is coupled to its pore-formation capacity and depends on its folding to the β-hairpin conformation (6). PG-1 is a very potent antibiotic peptide (7), and experimental NMR study has revealed the three-dimensional structure of PG-1 in solution (8).

The interaction of protegrin with the membrane strongly depends on its lipid composition. Recent experimental studies have shown that PG-1 inserts readily into a membrane composed of negatively charged anionic lipids with the phosphatidylglycerol (PG) headgroup but significantly less into a

Submitted February 24, 2006, and accepted for publication July 12, 2006.

Address reprint requests to Buyong Ma, Center for Cancer Research Nanobiology Program, SAIC-Frederick, Inc., NCI-Frederick, Frederick, MD 21702. Tel.: 301-846-6540; Fax: 301-846-5598; E-mail: mab@ncifcrf.gov.

© 2006 by the Biophysical Society

0006-3495/06/10/2848/12 $2.00

doi: 10.1529/biophysj.106.084046

membrane composed of neutrally charged lipids with the phosphatidylcholine (PC) or phosphatidylethanolamine (PE) headgroups (9). The major role of protegrins in the membrane is a channel formation that causes an ion leakage. Recently, it has been reported that either PG-1 or PG-3 can induce weak anion-selective channels and potassium leakage from liposomes and that PG-3 formed moderately cation-selective channels in the presence of bacterial lipopolysaccharide in planar phospholipid bilayers (10). Formation of protegrin channels disrupts the membrane surface by creating a pore across the membrane. Recent solid-state NMR has indicated that PG-1 is fully immersed in the lipid bilayer. The quantitative mismatch between the bilayer thickness and PG-1 length has suggested a local thinning of the bilayer (11,12). Experimental observations for α-helical peptides indicate that the thinning effect in the lipid bilayer is responsible for the formation of pores and/or channels in the membrane (13–16). PG-1 adopts a dimeric structure in DPC (dodecylphosphocholine) micelles, and a channel is formed by the association of several dimers (17).

The molecular mechanisms of the membrane damage caused by non-α-helical peptides are still unknown, and the structural basis for membrane disruption is not very apparent (18). Although recent computational efforts (19–23) mainly focus on the antimicrobial peptides revealing the peptide/lipid interaction, peptide insertion into membrane, and a membrane thinning effect, most of these investigations involve α-helical peptides. In this work, we performed extensive molecular dynamics (MD) simulations of the PG-1 monomer in explicit water, salt, and lipid bilayers composed of both homogeneous POPC lipids and a mixture of POPC/POPG (4:1) lipids. MD simulations of the peptide conformational change and the membrane interactions can provide information complementary to experimental approaches. Our long-term goal is to provide a detailed mechanism of the membrane-disrupting effects by cationic peptides with β-sheet structure. In this work we attempt to correlate the conformational change of the peptide and the membrane thinning effects by PG-1. In aqueous solution, the PG-1 monomer forms a more bent or collapsed structure with a loss of β-sheet content. In contrast, the β-hairpin is more planar at the amphipathic interface with the lipid bilayer. The conformational change indicates that the planar β-hairpin is the new structure adopted in the lipid-rich environments. Here, we observe membrane thinning effects for the PG-1 monomer/anionic membrane system, consistent with experimental observations. Further investigation of the PG-1 oligomerization effects on the enhancement of the membrane thinning is underway. We believe that this study provides insights into the first steps of the molecular mechanism of the membrane-disrupting effects by the peptide.

THEORETICAL CALCULATIONS

The PG-1 structure obtained from NMR spectroscopy (8) (Protein Data Bank numbers, 1PG1, model 14) was used for the all-atom simulations. The CHARMM program (24) and CHARMM 27 force field were used to construct the set of starting points within an explicit environment (including lipid bilayers, water, and salts) and to relax the systems to a production-ready stage. For production runs, the NAMD code (25) on a Biowulf cluster (26) at the National Institutes of Health (NIH) was used for the starting point with the same CHARMM 27 force field.

Building a unit cell containing a lipid bilayer

A unit cell containing two layers of lipids with almost 44,000 atoms is constructed. The β-hairpin structure of PG-1 used in the unit cell construction is the NMR structure. The peptide is initially located at the amphipathic region of the lipid bilayer on the extracellular side, with the two disulfide bonds facing the bilayer surface. The NMR structure was obtained in solution and does not provide any information regarding lipid molecules around the peptide. Our method closely follows a previous method, which has been successfully applied to gramicidin (27), α-helical systems (28,29), rhodopsin (30), bacteriorhodopsin (31), and fusion domain of influenza hemagglutinin (32). Our simulation employed the NPAT (constant number of atoms, pressure, surface area, and temperature) ensemble, an effective (time-averaged) surface tension, with a constant normal pressure applied in the direction perpendicular to the membrane. An alternative protocol would involve using variable surface area controlled by constant surface tension. However, although simulations with the NPγT (constant number of atoms, pressure, surface tension, and temperature) ensemble are useful when a peptide/protein is embedded in the lipid bilayer (33), in our case PG-1 is not fully inserted into the bilayer. Thus, since in the NPγT ensemble the precise value of the surface tension γ must be specified, in our case for such a heterogeneous lipid bilayer system γ is not known. For the membrane simulation, the observable macroscopic property of γ cannot directly estimate the value of γ for the microscopic membrane patch in the simulation (34). This has led us to use a constant surface area, since it has been shown that a simulation with an appropriate constant surface area can be directly comparable to an applied constant surface tension (34). In principle, holding the surface area and normal pressure constant may also present problems, since it may produce artifacts in the membrane thinning due to the confinement effect when the lipid bilayer begins to accommodate the peptide. However, the expected artifacts would be alleviated in our simulation, since PG-1 is only located at the amphipathic interface in the lipid bilayer. Spontaneous insertion of the peptide into the hydrophobic core is not observed due to the simulation timescale, which is not long enough to monitor a spontaneous insertion.

Two different types of lipid bilayers are constructed for the simulations. One is a homogeneous (or pure) lipid bilayer containing a single type of lipid molecule, POPC (palmitoyl-oleyl-phosphatidylcholine). The other is a heterogeneous (or mixed) lipid bilayer containing a mixture of lipid molecules, POPC and POPG (palmitoyl-oleyl-phosphatidylglycerol) with a ratio of POPC/POPG (4:1). The cross section areas per lipid for POPC and POPG are 63.5 Å^2 and 62.8 Å^2, respectively, as suggested by recent simulation studies (35). With a choice for the number of lipid molecules, the optimal value of lateral cell dimensions can be determined. For the pure lipid bilayer, 100 POPCs (50 POPCs each side) constitute the lateral cell dimension of 56.35 $\times$ 56.35 Å. For the mixed lipid bilayer, 80 POPCs and 20 POPGs (40 POPCs and 10 POPGs each side) constitute the lateral cell dimension of 56.3 $\times$ 56.3 Å. The bilayer thickness is defined by the distance between the average positions of the phosphorus atoms in two monolayers. Recent simulation studies reported that the bilayer thickness is 35.5 Å for the pure POPC lipid bilayer and 36.0 Å for the pure POPG lipid bilayer at a temperature of 310 K (35). We adopt a value of 35.5 Å for our POPC lipid bilayer and deduce a value of thickness of 35.6 Å for the mixed POPC/POPG (4:1) lipid bilayer. Rigid body dynamics, with constraints on the peptide backbone, was performed to obtain a better interfacial contact between the peptide and the lipid bilayer at the amphipathic interface.

A series of minimizations was performed to remove overlaps of the alkane chains and gradually relax the system. TIP3P waters were added and

relaxed through a series of minimization and dynamics. Six counterions (6 Cl^-) were inserted to electrically neutralize the pure lipid bilayer system, since there are six positively charged amino acid residues in the peptide. To obtain a physiological salt concentration near 100 mM, an additional 16 Na^+ and 16 Cl^- were added. The addition of explicit salt ions (more than charge-balancing counterions) to near-physiological conditions is required for reducing artifacts in the peptide conformation during the simulations (36,37). For the mixed lipid bilayer system, 14 Na^+ as counterions are inserted to neutralize the system (the system contains six positively charged residues and 20 anionic lipids). Also, 16 Na^+ and 16 Cl^- are added to get the same salt concentration. The initial placement of the ions is in the bulk water region, far from the peptide and the bilayer surfaces (37). For the two different lipid bilayer systems, many different initial configurations were constructed for the relaxation process. For each lipid bilayer simulation, the best initial configuration among more than two dozens initial configurations was selected as a starting point for the final production stage. The selection process is based on the criteria that all lipids should be distributed uniformly on the membrane surface and the lipid tails should be well ordered in the calculation of the lipid order parameter.

Building a unit cell for water box simulation

The simulations without lipid molecules are relatively simple. A cubic water box with cell dimensions of 50 × 50 × 50 Å was constructed with the peptide held at the origin. The β-hairpin structure of PG-1 from the NMR is also used for the unit cell construction. Six counterions (six Cl^-) were inserted to neutralize the system. In addition to the counterions, six Na^+ and six additional Cl^- were also added to get a salt concentration near 100 mM. Salts were initially put far from the peptide. A series of minimization and dynamics for the solvent were performed with the peptide held rigid. The system was then ready for the relaxation process.

Relaxation of initial configurations and production runs

The initial configurations were gradually relaxed, with the peptide held rigid. To relax the solvent, dynamic cycles were performed with electrostatic cutoffs (12 Å) and constant temperature (Nosé-Hoover). This ensures that all degrees of freedom were adjusted as much as possible before the peptide starts to move. In subsequent stages, the peptide was harmonically restrained, with the harmonic restraints gradually diminishing, allowing the peptide to adjust to the surrounding solvent. Harmonic restraints on the peptide backbone atoms were gradually relaxed until gone, with the dynamics performed on the NPAT ensemble. A Nosé-Hoover thermostat/barostat was used to maintain a constant temperature of 310 K for the lipid systems and 300 K for the water box and a constant pressure of 1 atm. Later equilibration stages include full Ewald electrostatics. Production runs of 10 ns for the starting points were performed on a Biowulf cluster (26) at NIH. Analysis was performed with the CHARMM programming package (24). Recent simulation studies suggest that ~10-ns duration simulations can reveal details of the interactions of lipid molecules with inner and outer membrane proteins (38,39).

RESULTS

Conformational dynamics of monomeric PG-1

The β-hairpin of PG-1 consists of 18 amino acid residues with a high content of Cys and Arg residues and is stabilized by two disulfide bonds between the Cys residues. Even with the two disulfide bonds, the monomeric PG-1 conformation is flexible. Experimentally, even though an NMR study revealed its refined three-dimensional structure in aqueous solution as consisting of a two-stranded antiparallel β-hairpin (8), the PG-1 conformation in the presence of micelles is better stabilized than in water (6,17). Our simulations are in agreement with the conformational behavior observed experimentally. Fig. 1 illustrates the simulated structures of PG-1 from the different environments. In the figure, all cartoons are in stereo view, representing (*a*) the NMR structure; (*b*) the final peptide conformation from the water box simulation, and snapshots at 1 ns, 5 ns, and 10 ns for the peptides from; (*c*) the pure bilayer system; and (*d*) the mixed bilayer system. In the cartoons, hydrophobic residues and disulfide-bonded Cys residues are shown in white, a polar residue (Tyr) and Gly are shown in green, and positively charged residues (Arg) are shown in blue. Disulfide bonds are highlighted in yellow. It can be clearly seen from the figure that the β-hairpin conformation is well retained in the presence of the lipid bilayers, although there is a slight conformational change from the NMR structure. In both lipid settings, the β-hairpins reorient the C-terminal β-strand, converting the overall β-hairpin to a cross β-sheet. The slightly bent β-strands found in the NMR structure become more elongated β-strands in the lipid setting.

In the bulky water environment, PG-1 becomes a bent structure (Fig. 1 *b*). Nevertheless, the two disulfide bonds hold the structure tightly; two strands locate near each other. The highly charged regions (turn and terminals) are highly flexible in the aqueous solution, whereas the hydrophobic core is relatively stable. The hydrophobic core, reinforced by the two disulfide bonds, provided the nuclei for the peptide to refold back to the regular β-hairpin structure once it meets a proper environment. The conformational differences in aqueous solution and membrane environment suggest a great structural plasticity of the PG-1 β-hairpin mediated by the lipid bilayer.

The details of the conformational flexibility of the PG-1 are plotted with the root mean squared deviations (RMSDs) relative to the starting point in Fig. 2 (averaged over the 10-ns simulations). The figure shows the RMSDs of C_α atoms of the peptide backbone (*upper*) and C_β atoms of the side chains (*lower panel*) for PG-1 in the water box (*open squares*), and on the surfaces of pure lipid bilayer (*inverted gray triangles*) and mixed lipid bilayer (*solid circles*). The starting point used for reference is a relaxed structure in the CHARMM potential, with minor changes from the NMR structure (8). Overall deviations that are very large (e.g., 5–10 Å or more) usually show an extremely flexible region. As expected, PG-1 in the water environment shows higher mobility than on both lipid bilayers, which is reflected in the larger deviation from the starting point, especially for both N- and C-termini and β-turn regions. In contrast, PG-1 in both lipid settings has smaller deviations from the starting point, indicating that its average position stays close to the starting point. The larger fluctuations in the RMSD of the C_β atoms as compared to those of the C_α atoms reflect the larger motions of the side chains. Note, however, that there are

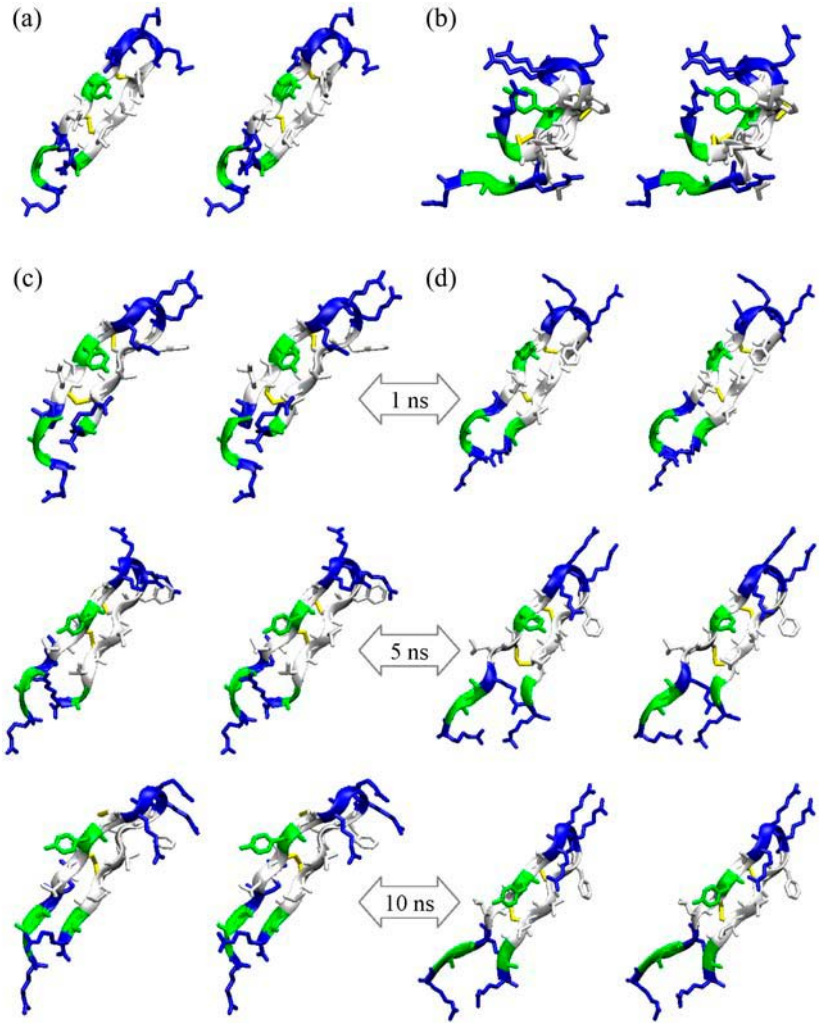

FIGURE 1 Cartoons of PG-1 in stereo view, representing (*a*) the NMR structure, (*b*) the final peptide conformation from the water box simulation, and snapshots at 1 ns, 5 ns, and 10 ns for the peptides from (*c*) the pure bilayer system and (*d*) the mixed bilayer system. In the cartoons, hydrophobic residues and disulfide-bonded Cys residues are shown in white, a polar residue (Tyr) and Gly are shown in green, and positively charged residues (Arg) are shown in blue. Disulfide bonds are highlighted in yellow.

significant motions in the Arg side chains of PG-1 in both lipid settings (residues 9–11) in the β-turn as compared to the corresponding backbone atoms. The active motions of the Arg side chains in the β-turn are associated with the interactions of the peptide at the amphipathic interface with the lipid bilayer and contribute to the membrane disruption effects of PG-1 (see results in the last subsection).

Energy partition of interaction between PG-1 and lipids

The interaction energy between the peptide and the surrounding environment is calculated to understand the dominant forces that stabilize the β-hairpin structure. This is performed every 10 ps over the 10-ns simulations. Fig. 3 *a* shows the resulting distributions of interaction energies for PG-1 in the water box (*upper part* of the figure) and for PG-1 on the surface of pure lipid bilayer (*middle*) and mixed lipid bilayer (*lower*). In the water box simulation, the interaction of PG-1 with water exhibits a typical bulky water interaction, since the distribution curve covers a wide range of interaction energies. However, in both lipid settings, the interactions of PG-1 with water and lipid exhibit distinct behavior, as indicated by the distribution peaks located above specific interaction energy levels. The interactions of PG-1 with the surrounding environments share common features in both lipid settings, showing that the distribution curve for the interaction of PG-1 with water is located at lower energy levels than that with lipid, which is much sharper. However, in contrast to these common features, PG-1 at the amphipathic interface in the mixed lipid bilayer has relatively stronger interactions with both water and lipid than that in the pure lipid bilayer, as indicated by the locations of distributions peaks at lower energy levels.

To investigate the contributions of each type of lipid to the total interaction energy for the mixed bilayer system, the distribution of the peptide interaction energy with lipid is separated into POPC and POPG lipid parts. Fig. 3 *b* shows the separated distributions of interaction energy with POPC (*upper panel*) and with POPG (*lower panel*) for PG-1 on the surface of the mixed lipid bilayer. The figure shows the distribution of the total interaction energy and the electrostatic

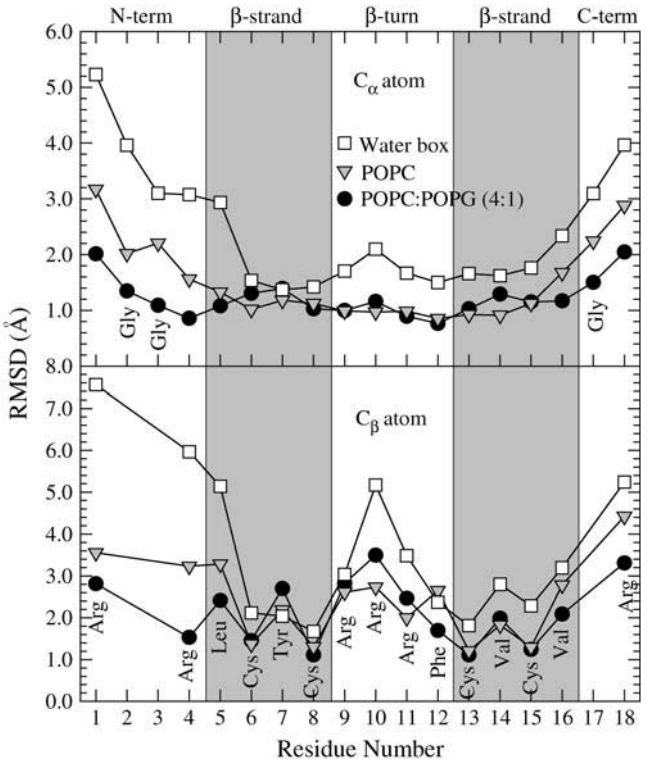

FIGURE 2 The average RMSD from the starting point for C_α atoms (*upper panel*) and C_β atoms (*lower panel*) of PG-1 in the water box (*open squares*), on the pure lipid bilayer composed of POPC (*inverted gray triangles*), and on the mixed lipid bilayer composed of POPC/POPG (4:1) (*solid circles*).

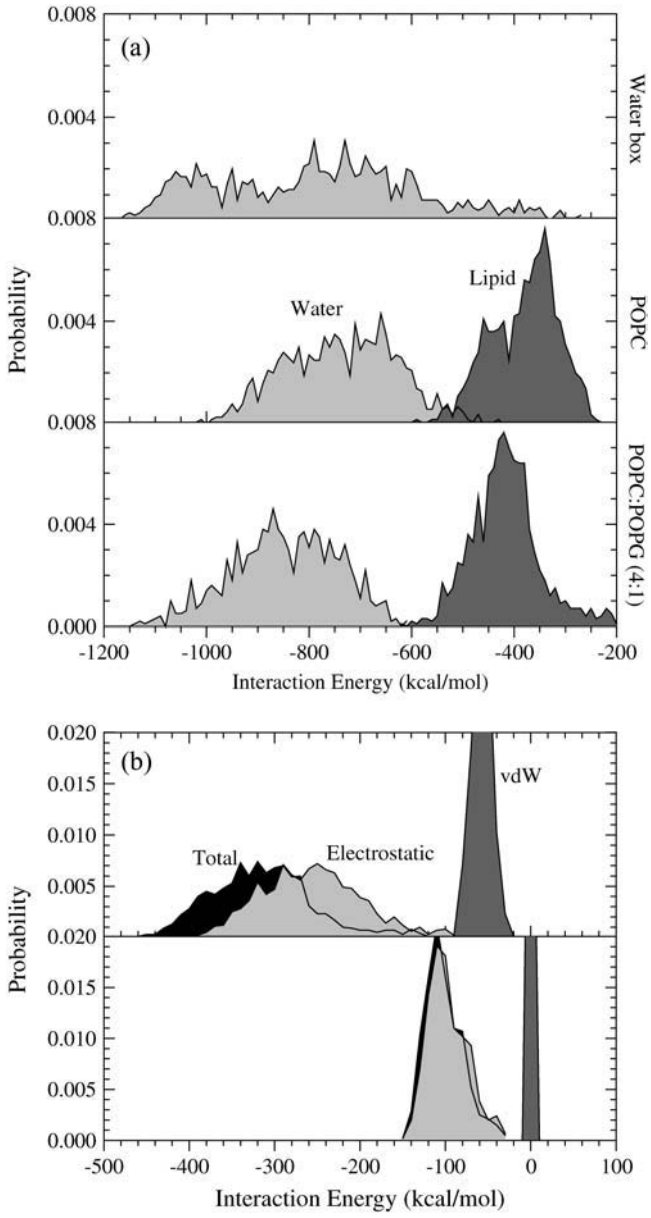

FIGURE 3 (*a*) Probability of interaction energies with the surrounding environments for PG-1 in the water box (*upper panel*), on the pure lipid bilayer composed of POPC (*middle panel*), and on the mixed lipid bilayer composed of POPC/POPG (4:1) (*lower panel*). (*b*) The interaction energy with the lipid is separated into POPC (*upper panel*) and POPG (*lower panel*) lipid parts for the mixed lipid bilayer system. The total interaction energies as well as the electrostatic contributions and the vdW contributions are shown.

and vdW contributions. The total interaction of PG-1 with POPC is the outcome of both the electrostatic and vdW interactions, whereas the total interaction of PG-1 with POPG derives dominantly from the contribution of the electrostatic interaction. In fact, the distribution of the total peptide interaction energy with POPC in the mixed lipid bilayer is qualitatively similar to that with lipid in the pure lipid bilayer, since the pure lipid bilayer is also composed of POPC. By comparing the distribution of peptide interaction energies with POPC, we observe a peak in the distribution curve located at 320 kcal/mol for the mixed lipid bilayer system (as in the *upper panel* of Fig. 3 *b*), which is similar to the peak location at 340 kcal/mol for the pure lipid bilayer system (as in the *middle panel* of Fig. 3 *a*). However, the interaction of PG-1 with lipid in the mixed lipid bilayer is relatively stronger than that in the pure lipid bilayer, since the peak in the distribution curve is located at 420 kcal/mol (the *bottom panel* of Fig. 3 *a*). As seen in the lower part of Fig. 3 *b*, 100 kcal/mol (mainly electrostatic interactions) of the peptide interaction energy with the lipid in the mixed lipid bilayer system derive from the peptide interaction energy with POPG.

It can be expected that in the presence of anionic lipids, electrostatic interactions may be the dominant force in the peptide/membrane system. A favorable attraction between the PG-1 peptide containing six positively charged residues and the negatively charged bilayer surface might bring the peptide close to the bilayer surface. Thus, we investigate the peptide's location with respect to the bilayer surface. Fig. 4 shows the time series of the peptide's center of mass displacement from the bilayer surface for the pure lipid bilayer (*black line*) and the mixed lipid bilayer (*gray line*) systems. The bilayer surface is defined as the average position of the phosphate atoms on the extracellular side. As expected, PG-1 on the surface of the mixed lipid bilayer is located closer to

the bilayer surface than on the pure lipid bilayer. This is consistent with the experimental observation that the ability of PG-1 to perturb and penetrate the anionic lipid bilayer is significantly enhanced compared to that of the zwitterionic lipid bilayer (9). This suggests that the interaction of the antimicrobial peptide PG-1 with the membrane strongly depends on the composition of lipid molecules in the membrane (21).

Membrane-disturbing effects by PG-1

Lipids play important roles in supporting the conformation and dynamics of PG-1 at the amphipathic interface of the lipid bilayer. The average positions of lipid groups and other solvent molecules may provide useful information regarding the environmental response to the peptide dynamics during the simulation. Fig. 5 *a* shows the position probability distribution functions (P) for five different component groups of POPC (*upper panel*), water, and salts (*lower panel*) as a function of the distance from the pure POPC lipid bilayer center. The POPC headgroup is divided into four subunits, choline (P_{Chol}, *black line*), phosphate (P_{PO4}, *red line*), glycerol (P_{Glyc}, *green line*), and carbonyl (P_{Carb}, *yellow line*). The tail group involves two fatty acids with terminal methyl (P_{CH3}, *blue line*). The peptide is located at the amphipathic region of the lipid bilayer on the extracellular side (positive z area), whereas the intracellular side (negative z area) contains lipids only. For the pure lipid bilayer system, the symmetric distributions of the lipid headgroups indicate that there are fewer disturbances in the lipid arrangement induced by the peptide. However, a small degree of disorder in the lipid tails is monitored as indicated by a plateau located at $z = 4$ Å in the P_{CH3} curve. In the distributions of salts, the probability for finding sodium ions near the bilayer surface at the intracellular side is high, whereas at the extracellular side a large number of chloride ions accumulate in the region next to the peptide.

The same position probability distribution functions (P) for the mixed lipid bilayer composed of POPC/POPG (4:1) is calculated by collecting data separated into POPC and POPG parts. Fig. 5 *b* shows position probability distribution functions (P) for five different component groups of POPC (*upper panel*) and POPG (*middle panel*), water, and salts (*lower panel*) as a function of the distance from the bilayer center for the mixed lipid. In POPG, a glycerol ($P_{\mathrm{Glyc}}^{\mathrm{Head}}$) subunit at the top of the lipid head replaces the choline subunit present in POPC. The peptide induces an asymmetry in the distribution of POPC headgroups. It can be seen that the POPC headgroups on the extracellular side are distributed along the membrane normal more widely than those on the intracellular side. In the distribution of POPG headgroups, disordered arrangements of POPG heads are observed on both sides of the bilayer. We observed lipids with significantly disordered tails, especially those in contact with the peptide (see below). We suspect that the disordering of lipid tails causes the thinning of the lipid bilayer. In the distribution of salts, compared to the pure bilayer system, the probability of sodium ions near the bilayer surface at the intracellular side is very high due to the strong electrostatic attraction between sodium ions and the anionic lipids in the bilayer. On the extracellular side, the probability of sodium ions is smaller, indicating that the presence of the peptide on the bilayer surface reduces the sodium attraction. Chloride ions at the extracellular side are repelled from the bilayer surface, since the peptide/bilayer system still has a net negative charge.

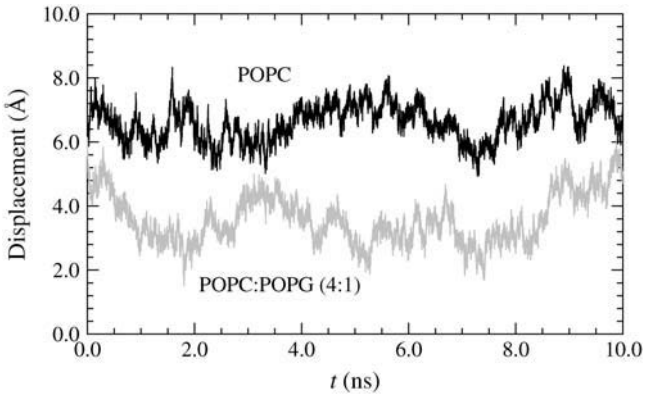

FIGURE 4 Time series of peptide displacement from the average position of phosphate atoms on the extracellular side for PG-1 on the pure lipid bilayer composed of POPC (*black line*) and the mixed lipid bilayer composed of POPC/POPG (4:1) (*gray line*).

Water molecules in the mixed lipid bilayer behave differently compared to those in the pure lipid bilayer. In Fig. 5 *c*, the position probability distribution function for water, P_{water}, is highlighted to compare the differences between the pure lipid bilayer (*red*) and the mixed lipid bilayer (*blue*) systems. On the intracellular side, the probability curves for water reduce to zero at $z = -9$ Å for both bilayer systems. However, on the extracellular side more water molecules penetrate into the hydrophobic region in the mixed lipid bilayer. The large number of water molecules penetrating the mixed lipid bilayer can characterize the complex amphipathic dynamics between the peptide and the lipid bilayer and the thinning pathway.

To investigate the average structure in the interior of the bilayer, the deuterium order parameter, S_{CD}, was calculated using $S_{\mathrm{CD}} = \frac{1}{2}\langle 3\cos^2\theta - 1\rangle$, where θ is the angle between the C-H bond vector and the membrane normal, and the angular brackets indicate averaging over time and over lipids. Fig. 6 shows the order parameters for the oleoyl (*left column*) and palmitoyl (*right*) chains for the pure lipid bilayer composed of POPC (all *circles*) and the mixed lipid bilayer composed of POPC/POPG (4:1) (all *triangles*). Lipids in the extracellular (peptide-containing) (*upper panel*) and intracellular (*lower*) sides are considered separately. On the extracellular side, lipids are further divided into two categories: local (those adjacent to the peptide) and bulk (all others) lipids. The local lipids are denoted by open symbols (*open circles* and *triangles*), and the bulk lipids are denoted by filled

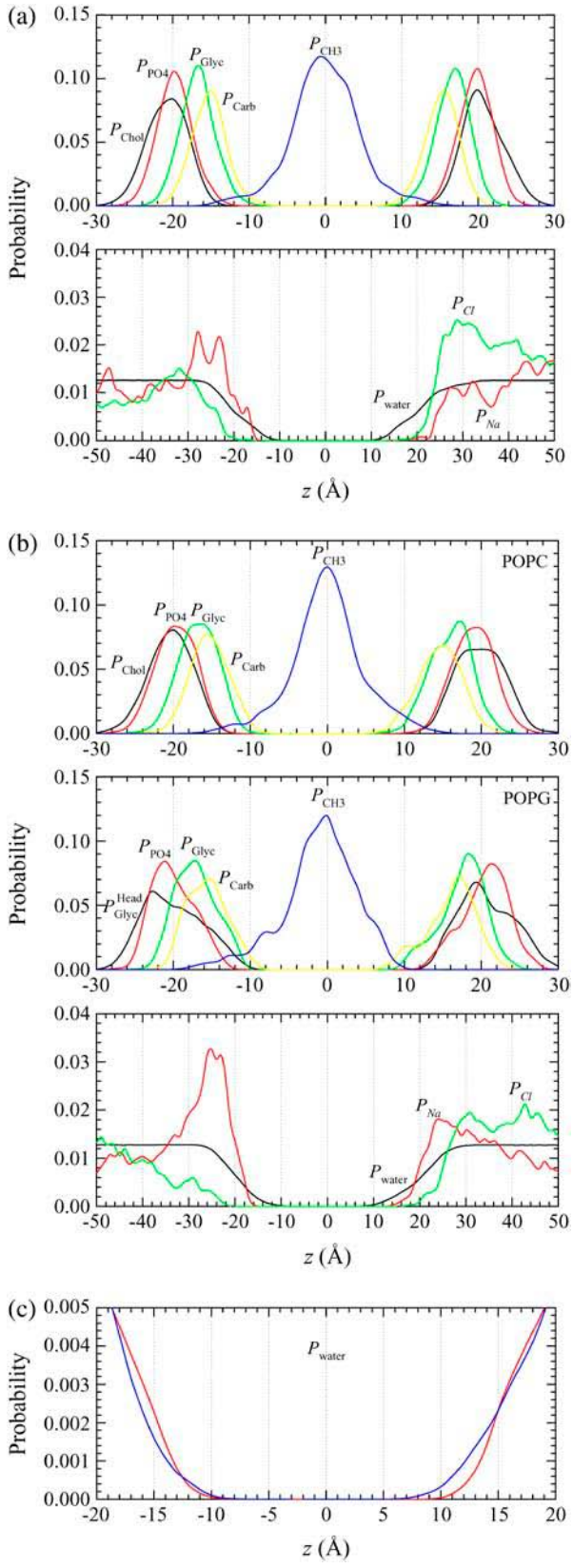

FIGURE 5 (*a*) Probability distribution functions (*P*) for different component groups of lipid (P_{Chol} (choline), P_{PO4} (phosphate), P_{Glyc} (glycerol), P_{Carb} (carbonyls), and P_{CH3} (methyl)) and for other solvents (P_{water} (water), P_{Na} (sodium ion), and P_{Cl} (chloride ion)) as a function of distance from the bilayer center for PG-1 on the pure lipid bilayer composed of POPC. (*b*) The same probability distribution functions for PG-1 on the mixed lipid bilayer composed of POPC/POPG (4:1). The probability distribution functions are separated into POPC (*upper panel*) and POPG (*middle panel*) lipid parts. In the distribution function for POPG, P_{Chol} (choline) from POPC is replaced by P^{Head}_{Glyc} (top-head glycerol). (*c*) Highlight of the probability distribution function for water, P_{water}, for the pure lipid bilayer (*red*), and for the mixed lipid bilayer systems (*blue*). PG-1 is located at the lipid/water interface in the positive *z* region.

symbols (*solid circles* and *gray triangles*). The bars represent the standard errors. For both oleoyl and palmitoyl chains of the bulk lipids, the order parameters for both pure and mixed lipid bilayers are qualitatively similar to each other. On the extracellular side, the order parameters for the local lipids in both bilayers are significantly less than those for the bulk lipids. Note, however, that the order parameters for the local lipids in the mixed bilayer are much less than those in the pure bilayer, indicating that the local lipids in the mixed bilayer have significantly disordered tails that cause the thinning of the lipid bilayer.

A striking effect of membrane disruption under the peptide invasion is revealed by analyzing the average position of lipids on the bilayer surface during the simulation. Fig. 7 shows the average positions of the center of mass of each of the extracellular half lipids on the *x-y* plane that can be defined as a projection of the bilayer surface. The contour lines enclose highly populated center of mass positions of each POPC (*gray lines*) and POPG (*black lines*) on the extracellular side. The peptide is also projected onto the plane as an average structure with its average position during the simulation. For the pure lipid bilayer system in Fig. 7 *a*, all lipids are distributed isotropically on the plane. On the other hand, for the mixed lipid bilayer system in Fig. 7 *b*, a significant deficiency in the distribution of the locations of the lipids' center of mass is evident from the wide empty space underneath the β-turn of PG-1. This is compelling evidence for the capability of PG-1 to disrupt/thin the membrane. In the presence of anionic lipids, PG-1 is located closer to the bilayer surface as seen in Fig. 4. In the deep amphipathic region, the Arg residues in the β-turn stretch their long side chains parallel to the bilayer surface, easily pushing the bottom of the lipid heads which are closer to the lipids' center of mass. The side chains interact strongly with the lipid heads located around the β-turn, in a way that the lipid heads tilt in the direction of the Arg side chain and the lipids' center of mass shifts to the end of the side chains. This leads to an absence of the lipids' center of mass around the β-turn. Consequently, the lipid bilayer exposes a hydrophobic bath to the peptide; and the hydrophobic residue Phe, at the end of the β-turn, can easily immerse into this bath. Immersion of the hydrophobic side chain of Phe causes the conformational change of PG-1 shown in Fig. 1, in which the C-terminal β-strand is reoriented. We note that although the hydrophobic side chains' immersion and the reorientation of the

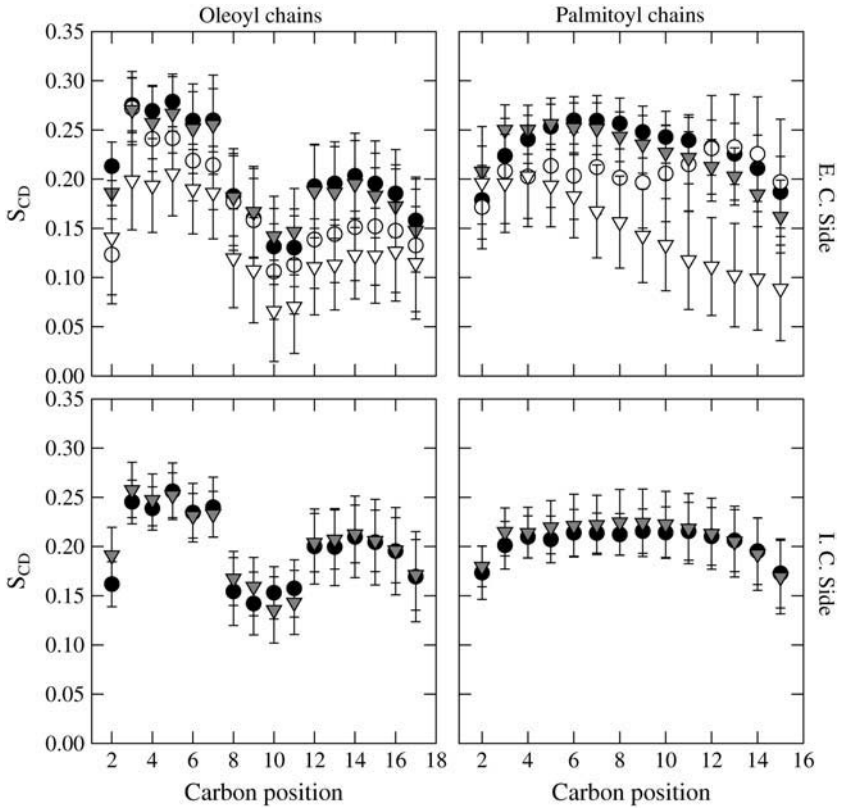

FIGURE 6 Deuterium order parameters, S_{CD}, for the oleoyl (*left column*) and palmitoyl (*right*) chains for the different lipid categories, for the extracellular (peptide-containing) side (*upper panel*) and the intracellular (*lower*) side, and for the pure lipid bilayer composed of POPC (*all circles*) and the mixed lipid bilayer composed of POPC/POPG (4:1) (*all triangles*). The local lipids (those adjacent to the peptide) are denoted by open symbols (*open circles* and *triangles*), and the bulk lipids are denoted by filled symbols (*solid circles* and *gray triangles*).

C-terminal β-strand are also monitored for PG-1 on the pure lipid bilayer, it is only on the mixed lipid bilayer that the peptide causes the local lipid integration/dissociation that is directly responsible for the bilayer thinning.

To further analyze the thinning effect mediated by PG-1, the three-dimensional densities for the positions of the lipid headgroups are calculated during the 10-ns simulation. Fig. 8 shows the three-dimensional density maps of the lipid headgroups for (*a*) the pure lipid bilayer, and (*b*) the mixed lipid bilayers. In Fig. 8, *a* and *b*, the upper figure is a top view from the extracellular side with an embedded peptide, and the lower figure is a lateral view of the bilayer. The blue line in the lower figure connects the three midpoints of the headgroup map, indicating the degree of the bilayer bending. The vertical double arrow in the lower figure points to the degree of the bilayer thickness. The headgroup density map reflects the average shape of the bilayer surface during the simulation. The pure lipid bilayer in Fig. 8 *a* indicates some roughness of the bilayer surface. In the lateral view of the bilayer, the three-point connection shows no symptom of a bending of the bilayer surface. For the mixed bilayer in Fig. 8 *b*, the roughness of the bilayer surface becomes clearer. Furthermore, we observe that there is a dent or hole in the surface in the large area below the β-turn. The location of the dent in the bilayer surface is consistent with the location of the empty space in Fig. 7 *b*. The dent begins to appear after 2 ns from the start of the simulation and is stable afterward. In the lateral view of the bilayer, the three-point connection clearly indicates that there is significant bending of the extracellular surface. The bending of the bilayer surface is closely related with the membrane thinning effect. The vertical double arrow indicates a thinning of the bilayer. Compared with the pure lipid bilayer, the thickness of the mixed lipid bilayer is much smaller, particularly underneath the peptide.

The density map calculations also give us useful information on the exact interaction sites around the peptide by the solvent including water and ions. Fig. 9 shows the density maps of water (*blue*), sodium (*yellow*), and chloride (*white*) ions for PG-1 on the pure lipid bilayer (*upper panel*) and the mixed lipid bilayer (*lower panel*). The average structures of the peptide during the 10-ns simulation are presented in the figure with color codes as follows: blue—positively charged residue, white—hydrophobic, and green—polar residue. An isomesh encloses the same probability values in space, and an isosurface encloses higher probability values than the isomesh. For PG-1 on the pure bilayer, water solvation sites with probabilities of 0.4/0.5 (mesh/surface) are observed around the peptide. Popular chloride interaction sites with probabilities of 0.02/0.03 (mesh/surface) around the β-turn indicate that the Arg side chains have strong electrostatic interactions with chloride ions. Sodium interaction sites with probabilities of 0.01 (mesh) are relatively rare. For PG-1 on the mixed bilayer, water solvation sites with probabilities of 0.4/0.5 (mesh/surface), chloride interaction sites with probabilities of 0.015/0.02 (mesh/surface), and sodium interaction sites with probabilities of 0.015/0.02 (mesh/

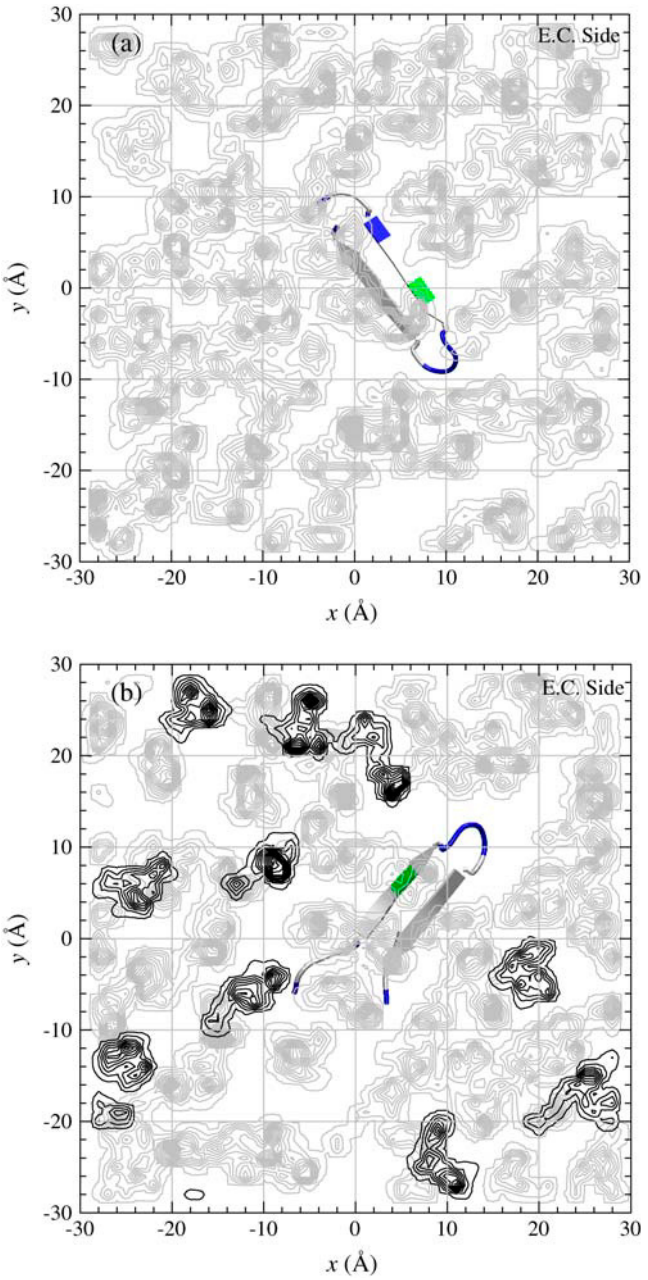

FIGURE 7 Mapping of x, y coordinates of the center of mass of each lipid on the extracellular half lipids onto the x-y plane for (*a*) the pure lipid bilayer composed of POPC and (*b*) the mixed lipid bilayer composed of POPC/POPG (4:1). The contour lines enclose highly populated locations of the center of mass of each POPC (*gray lines*) and POPG (*black lines*). The peptide is also projected onto the plane as an average structure with its average position during the simulation. Hydrophobic residues including Gly and disulfide-bonded Cys residues are shown in white, a polar residue (Tyr) is shown in green, and positively charged residues (Arg) are shown in blue.

surface) are observed. Compared with the pure bilayer system, chloride interaction sites around the β-turn are reduced in the mixed bilayer system. Here, the chloride ions are repelled from the bilayer surface due to the negative nature of the lipid interface/peptide system. This suggests that the Arg side chains interact more with lipid molecules in the mixed bilayer. In other words, the interactions of the Arg side chains with lipid molecules in the pure bilayer system are screened by chloride ions. This can explain partly the fact that PG-1 interaction with the lipid bilayer is enhanced in the presence of negatively charged lipids in the membrane.

DISCUSSION

We simulated the PG-1 monomer in different environments: an explicit water box containing salts, pure lipid bilayer composed of POPC, and a mixed lipid bilayer composed of POPC/POPG (4:1). In our simulations, the bulk water environment does not support the β-hairpin structure of PG-1 that was defined from NMR spectroscopy (8). However, in both lipid bilayer settings the β-hairpin structure of PG-1 is well preserved. In addition, PG-1 adapts to the new lipid-rich environments through a structural rearrangement in the C-terminal β-strand. Importantly, the new PG-1 conformation at the amphipathic interface with the lipid bilayer implies that PG-1 is ready to conduct its physiological activity in the membrane. PG-1 is known as a membrane-damaging peptide with a great antibiotic potency (7). PG-1 activity is strongly supported by its stable β-hairpin conformation (2). Although PG-1 loses its β-hairpin motif by breaking the β-sheet H-bonds in a bulk water environment, the two disulfide S-S bonds in PG-1 hold the structure tightly, indicating that the β-hairpin motif can be easily recovered through the formation of β-sheet H-bonds in a proper environment. This large conformational flexibility of PG-1 due to the disulfide bonds is effectuated at the amphipathic interface in the lipid bilayer. The disulfide bonds in the stable β-hairpin PG-1 are partly responsible for the membrane thinning effect, since they form a hydrophobic cluster in the middle of the β-hairpin, perturbing the polar lipid heads at the amphipathic interface.

The detailed mechanisms of the membrane disruption, especially those caused by β-sheet peptides, are still unclear (18). In this work, our attention focuses on the conformational change of PG-1 at the amphipathic interface of the lipid bilayer and on the bilayer thinning by the peptide. PG-1 shares a common conformation at the amphipathic interface of the bilayer, and the structure differs from the solution NMR structure (8). The solution NMR structure is a slightly bent β-hairpin, but it changes to a planar β-hairpin at both lipid settings with the same number of intramolecular H-bonds as in the NMR structure. However, PG-1 exhibits different features at the interface of lipid bilayers with different lipid compositions. In the presence of anionic lipids in the bilayer, PG-1 locates more closely to the bilayer surface and interacts more strongly with the lipids, although the peptide has the same initial distance from the bilayer surface in the starting points of both lipid bilayers. As suggested by experimental observations, the electrostatic interactions between the positive charges of antimicrobial peptide and acidic headgroups of lipid play an important role in the peptide/

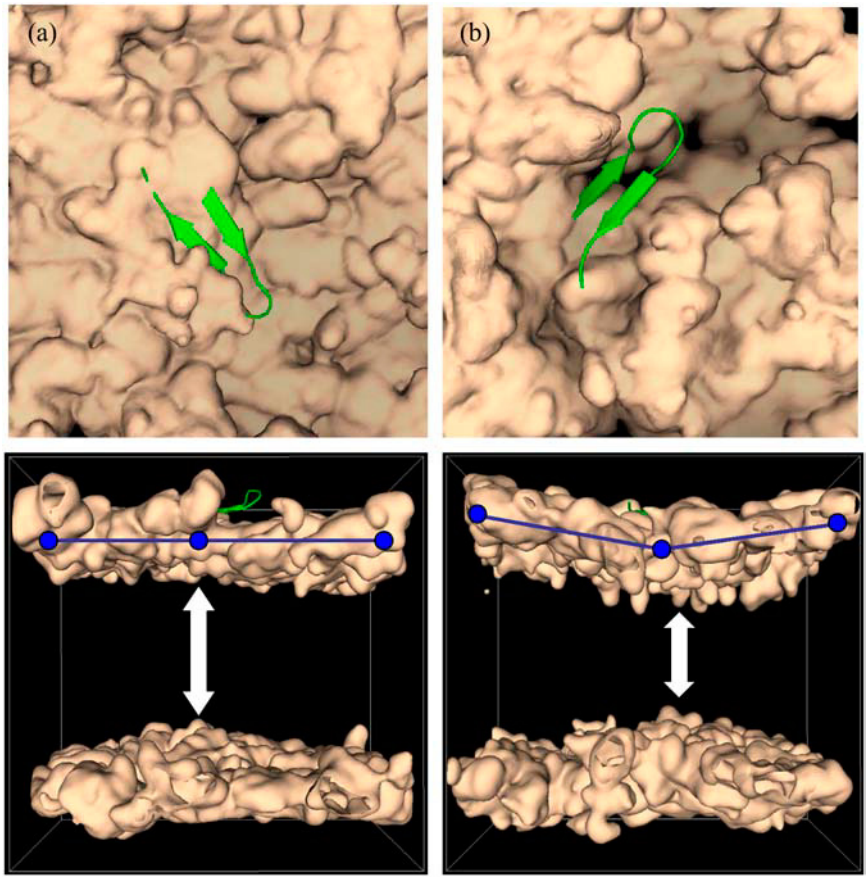

FIGURE 8 Three-dimensional density maps of the lipid headgroup for (*a*) the pure lipid bilayer composed of POPC and (*b*) the mixed lipid bilayer composed of POPC/POPG (4:1). In both figures, the upper figure is the top view from the extracellular side with an embedded peptide and the lower figure is the lateral view of the bilayer. In the lateral bilayer views, the blue lines are the three-point connection that measures the bilayer bending, and the vertical double arrow points the degree of the bilayer thickness. Note that the three points and lines are only guides to eyes.

lipid interaction (40,41), indicating that most antimicrobial peptides have a great tendency to locate at the amphipathic interface of the bilayer (42–44). Local thinning of the lipid bilayer due to the PG-1 invasion is clearer in the lipid bilayer with anionic lipids, which is consistent with experimental observation (9). Results of recent simulations also indicate that PG-1 interacts more strongly with an anionic micelle than a zwitterionic micelle, supporting the disruption of membrane (45). The Arg residues in the β-hairpin turn region are found to be mostly responsible for the local thinning effect in the mixed lipid bilayer. In the anionic lipid setting, the peptide conformational change followed by its function in a membrane environment is closely related to the mechanism of the membrane thinning effect.

In our simulation, lateral hopping between lipid molecules was not observed, since the timescale for such two-dimensional diffusion ranges from a few hundred nanoseconds to a microsecond, which is far beyond the timescale of our simulations. Thus the anionic lipids did not exchange their positions to condense around the cationic peptide. However the peptide is very mobile, indicating that the peptide can easily slip into the local energy minimum site. At the starting points of both lipid simulations, all lipids were distributed uniformly on the membrane surface, and after the complete preequilibration stage (details are provided in the Theoretical Calculations section), no deficiency in the lateral distribution of the lipids was observed before the production runs. Hence, our simulation results are not affected by the initial distribution of the lipid molecules. We note however that for the mixed lipid bilayer, different arrangements of the anionic lipid around the peptide may alter the final peptide conformation. Nevertheless, the effect is very subtle, and hence does not affect the trend observed here.

Our simulation results provide important guidelines for how the environment supports the PG-1 conformation and how the PG-1 activity adapts to the environment. Although the PG-1 monomer indeed induces local thinning of the lipid bilayer with anionic lipids, the membrane-disrupting effects such as pore/channel formation are directly mediated by packing of PG-1 dimers into ordered aggregates (17,46,47). Recent experimental studies demonstrate that the solid-state aggregation of PG-1 is consistent with its ordered aggregation in bilayers (46,47). Further investigations of the PG-1 dimers in different intermolecular packing and in different settings of the lipid bilayers are being conducted to further our understanding of the complex behavior of membrane disruption.

This study utilized the high-performance computational capabilities of the Biowulf PC/Linux cluster at the National Institutes of Health, Bethesda, MD (http://biowulf.nih.gov).

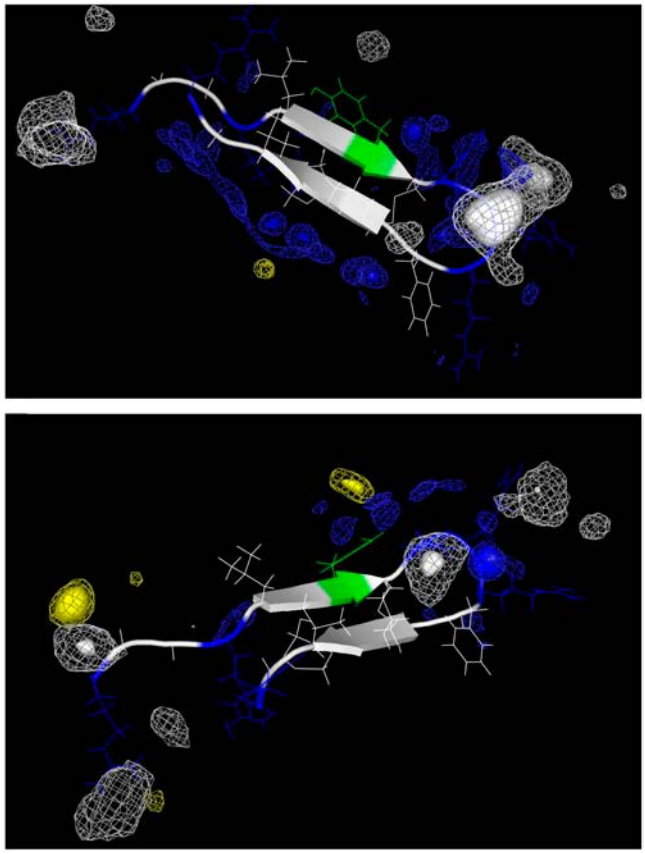

FIGURE 9 Three-dimensional density map of water (*blue*), sodium (*yellow*), and chloride (*white*) ions for the pure lipid bilayer composed of POPC (*upper*) and the mixed lipid bilayer composed of POPC/POPG (4:1) (*lower*). In the peptide, hydrophobic residues including Gly and disulfide-bonded Cys residues are shown in white, a polar residue (Tyr) is shown in green, and positively charged residues (Arg) are shown in blue.

This project was funded in whole or in part by the U.S. Army Medical Research Acquisition Activity under grant W81XWH-05-1-0002 and with federal funds from the National Cancer Institute, National Institutes of Health (NIH), under contract number NO1-CO-12400. This research was supported (in part) by the Intramural Research Program of the NIH, National Cancer Institute, Center for Cancer Research.

REFERENCES

1. Kourie, J. I., and A. A. Shorthouse. 2000. Properties of cytotoxic peptide-formed ion channels. *Am. J. Physiol. Cell Physiol.* 278:C1063–C1087.
2. Lai, J. R., B. R. Huck, B. Weisblum, and S. H. Gellman. 2002. Design of non-cysteine-containing antimicrobial β-hairpins: structure-activity relationship studies with linear protegrin-1 analogues. *Biochemistry.* 41:12835–12842.
3. Gobbo, M., L. Biondi, F. Filira, R. Gennaro, M. Benincasa, B. Scolaro, and R. Rocchi. 2002. Antimicrobial peptides: synthesis and antibacterial activity of linear and cyclic drosocin and apidaecin 1b analogues. *J. Med. Chem.* 45:4494–4504.
4. Panchal, R. G., M. L. Smart, D. N. Bowser, D. A. Williams, and S. Petrou. 2002. Pore-forming proteins and their application in biotechnology. *Curr. Pharm. Biotechnol.* 3:99–115.
5. Sitaram, N., and R. Nagaraj. 1999. Interaction of antimicrobial peptides with biological and model membranes: structural and charge requirements for activity. *Biochim. Biophys. Acta.* 1462:29–54.
6. Drin, G., and J. Temsamani. 2002. Translocation of protegrin I through phospholipid membranes: role of peptide folding. *Biochim. Biophys. Acta.* 1559:160–170.
7. Miyasaki, K. T., and R. I. Lehrer. 1998. β-sheet antibiotic peptides as potential dental therapeutics. *Int. J. Antimicrob. Agents.* 9:269–280.
8. Fahrner, R. L., T. Dieckmann, S. S. Harwig, R. I. Lehrer, D. Eisenberg, and J. Feigon. 1996. Solution structure of protegrin-1, a broad-spectrum antimicrobial peptide from porcine leukocytes. *Chem. Biol.* 3:543–550.
9. Gidalevitz, D., Y. Ishitsuka, A. S. Muresan, O. Konovalov, A. J. Waring, R. I. Lehrer, and K. Y. Lee. 2003. Interaction of antimicrobial peptide protegrin with biomembranes. *Proc. Natl. Acad. Sci. USA.* 100:6302–6307.
10. Sokolov, Y., T. Mirzabekov, D. W. Martin, R. I. Lehrer, and B. L. Kagan. 1999. Membrane channel formation by antimicrobial protegrins. *Biochim. Biophys. Acta.* 1420:23–29.
11. Buffy, J. J., T. Hong, S. Yamaguchi, A. J. Waring, R. I. Lehrer, and M. Hong. 2003. Solid-state NMR investigation of the depth of insertion of protegrin-1 in lipid bilayers using paramagnetic Mn^{2+}. *Biophys. J.* 85:2363–2373.
12. Yamaguchi, S., T. Hong, A. Waring, R. I. Lehrer, and M. Hong. 2002. Solid-state NMR investigations of peptide-lipid interaction and orientation of a β-sheet antimicrobial peptide, protegrin. *Biochemistry.* 41:9852–9862.
13. Chen, F. Y., M. T. Lee, and H. W. Huang. 2003. Evidence for membrane thinning effect as the mechanism for peptide-induced pore formation. *Biophys. J.* 84:3751–3758.
14. Zakharov, S. D., E. A. Kotova, Y. N. Antonenko, and W. A. Cramer. 2004. On the role of lipid in colicin pore formation. *Biochim. Biophys. Acta.* 1666:239–249.
15. Mecke, A., D. K. Lee, A. Ramamoorthy, B. G. Orr, and M. M. Banaszak Holl. 2005. Membrane thinning due to antimicrobial peptide binding: an atomic force microscopy study of MSI-78 in lipid bilayers. *Biophys. J.* 89:4043–4050.
16. Allende, D., S. A. Simon, and T. J. McIntosh. 2005. Melittin-induced bilayer leakage depends on lipid material properties: evidence for toroidal pores. *Biophys. J.* 88:1828–1837.
17. Roumestand, C., V. Louis, A. Aumelas, G. Grassy, B. Calas, and A. Chavanieu. 1998. Oligomerization of protegrin-1 in the presence of DPC micelles. A proton high-resolution NMR study. *FEBS Lett.* 421:263–267.
18. Bechinger, B. 2000. Understanding peptide interactions with the lipid bilayer: a guide to membrane protein engineering. *Curr. Opin. Chem. Biol.* 4:639–644.
19. Berneche, S., M. Nina, and B. Roux. 1998. Molecular dynamics simulation of melittin in a dimyristoylphosphatidylcholine bilayer membrane. *Biophys. J.* 75:1603–1618.
20. Shepherd, C. M., H. J. Vogel, and D. P. Tieleman. 2003. Interactions of the designed antimicrobial peptide MB21 and truncated dermaseptin S3 with lipid bilayers: molecular-dynamics simulations. *Biochem. J.* 370:233–243.
21. Lensink, M. F., B. Christiaens, J. Vandekerckhove, A. Prochiantz, and M. Rosseneu. 2005. Penetratin-membrane association: W48/R52/W56 shield the peptide from the aqueous phase. *Biophys. J.* 88:939–952.
22. Kandasamy, S. K., and R. G. Larson. 2005. Molecular dynamics study of the lung surfactant peptide SP-B1-25 with DPPC monolayers: insights into interactions and peptide position and orientation. *Biophys. J.* 88:1577–1592.
23. Appelt, C., F. Eisenmenger, R. Kuhne, P. Schmieder, and J. A. Soderhall. 2005. Interaction of the antimicrobial peptide cyclo(RRWWRF) with membranes by molecular dynamics simulations. *Biophys. J.* 89:2296–2306.
24. Brooks, B. R., R. E. Bruccoleri, B. D. Olafson, D. J. States, S. Swaminathan, and M. Karplus. 1983. CHARMM—a program for macromolecular energy, minimization, and dynamics calculations. *J. Comput. Chem.* 4:187–217.

25. Phillips, J. C., R. Braun, W. Wang, J. Gumbart, E. Tajkhorshid, E. Villa, C. Chipot, R. D. Skeel, L. Kale, and K. Schulten. 2005. Scalable molecular dynamics with NAMD. *J. Comput. Chem.* 26:1781–1802.

26. National Institutes of Health. Biowulf at the NIH. http://biowulf.nih.gov. [Online].

27. Woolf, T. B., and B. Roux. 1994. Molecular dynamics simulation of the gramicidin channel in a phospholipid bilayer. *Proc. Natl. Acad. Sci. USA.* 91:11631–11635.

28. Woolf, T. B. 1997. Molecular dynamics of individual alpha-helices of bacteriorhodopsin in dimyristol phosphatidylocholine. I. Structure and dynamics. *Biophys. J.* 73:2376–2392.

29. Woolf, T. B. 1998. Molecular dynamics simulations of individual alpha-helices of bacteriorhodopsin in dimyristoylphosphatidylcholine. II. Interaction energy analysis. *Biophys. J.* 74:115–131.

30. Crozier, P. S., M. J. Stevens, L. R. Forrest, and T. B. Woolf. 2003. Molecular dynamics simulation of dark-adapted rhodopsin in an explicit membrane bilayer: coupling between local retinal and larger scale conformational change. *J. Mol. Biol.* 333:493–514.

31. Jang, H., P. S. Crozier, M. J. Stevens, and T. B. Woolf. 2004. How environment supports a state: molecular dynamics simulations of two states in bacteriorhodopsin suggest lipid and water compensation. *Biophys. J.* 87:129–145.

32. Lagüe, P., B. Roux, R. W. Pastor. 2005. Molecular dynamics simulations of the influenza hemagglutinin fusion peptide in micelles and bilayers: conformational analysis of peptide and lipids. *J. Mol. Biol.* 354:1129–1141.

33. Zhang, Y. H., S. E. Feller, B. R. Brooks, and R. W. Pastor. 1995. Computer simulation of liquid/liquid interfaces. 1. Theory and application to octane/water. *J. Chem. Phys.* 103:10252–10266.

34. Feller, S. E., and R. W. Pastor. 1999. Constant surface tension simulations of lipid bilayers: the sensitivity of surface areas and compressibilities. *J. Chem. Phys.* 111:1281–1287.

35. Rog, T., K. Murzyn, and M. Pasenkiewicz-Gierula. 2003. Molecular dynamics simulations of charged and neutral lipid bilayers: treatment of electrostatic interactions. *Acta Biochim. Pol.* 50:789–798.

36. Ibragimova, G. T., and R. C. Wade. 1998. Importance of explicit salt ions for protein stability in molecular dynamics simulation. *Biophys. J.* 74:2906–2911.

37. Pfeiffer, S., D. Fushman, and D. Cowburn. 1999. Impact of Cl^- and Na^+ ions on simulated structure and dynamics of βARK1 PH domain. *Proteins.* 35:206–217.

38. Deol, S. S., P. J. Bond, C. Domene, and M. S. Sansom. 2004. Lipid-protein interactions of integral membrane proteins: a comparative simulation study. *Biophys. J.* 87:3737–3749.

39. Domence, C., P. J. Bond, S. S. Deol, and M. S. P. Sansom. 2003. Lipid/protein interactions and the membrane/water interfacial region. *J. Am. Chem. Soc.* 125:14966–14967.

40. Gazit, E., A. Boman, H. G. Boman, and Y. Shai. 1995. Interaction of the mammalian antibacterial peptide cecropin P1 with phospholipid vesicles. *Biochemistry.* 34:11479–11488.

41. Gazit, E., W. J. Lee, P. T. Brey, and Y. Shai. 1994. Mode of action of the antibacterial cecropin B2: a spectrofluorometric study. *Biochemistry.* 33:10681–10692.

42. Glaser, R. W., C. Sachse, U. H. Durr, P. Wadhwani, S. Afonin, E. Strandberg, and A. S. Ulrich. 2005. Concentration-dependent realignment of the antimicrobial peptide PGLa in lipid membranes observed by solid-state 19F-NMR. *Biophys. J.* 88:3392–3397.

43. Yamaguchi, S., D. Huster, A. Waring, R. I. Lehrer, W. Kearney, B. F. Tack, and M. Hong. 2001. Orientation and dynamics of an antimicrobial peptide in the lipid bilayer by solid-state NMR spectroscopy. *Biophys. J.* 81:2203–2214.

44. Marassi, F. M., S. J. Opella, P. Juvvadi, and R. B. Merrifield. 1999. Orientation of cecropin A helices in phospholipid bilayers determined by solid-state NMR spectroscopy. *Biophys. J.* 77:3152–3155.

45. Langham, A. A., H. Khandelia, and Y. N. Kaznessis. 2006. How can a β-sheet peptide be both a potent antimicrobial and harmfully toxic? Molecular dynamics simulations of protegrin-1 in micelles. *Biopolymers.* 84:219–231.

46. Buffy, J. J., A. J. Waring, and M. Hong. 2005. Determination of peptide oligomerization in lipid bilayers using 19F spin diffusion NMR. *J. Am. Chem. Soc.* 127:4477–4483.

47. Tang, M., A. J. Waring, and M. Hong. 2005. Intermolecular packing and alignment in an ordered β-hairpin antimicrobial peptide aggregate from 2D solid-state NMR. *J. Am. Chem. Soc.* 127:13919–13927.